Energy & Environmental Science

www.rsc.org/ees

Volume 3 | Number 2 | February 2010 | Pages 165–240

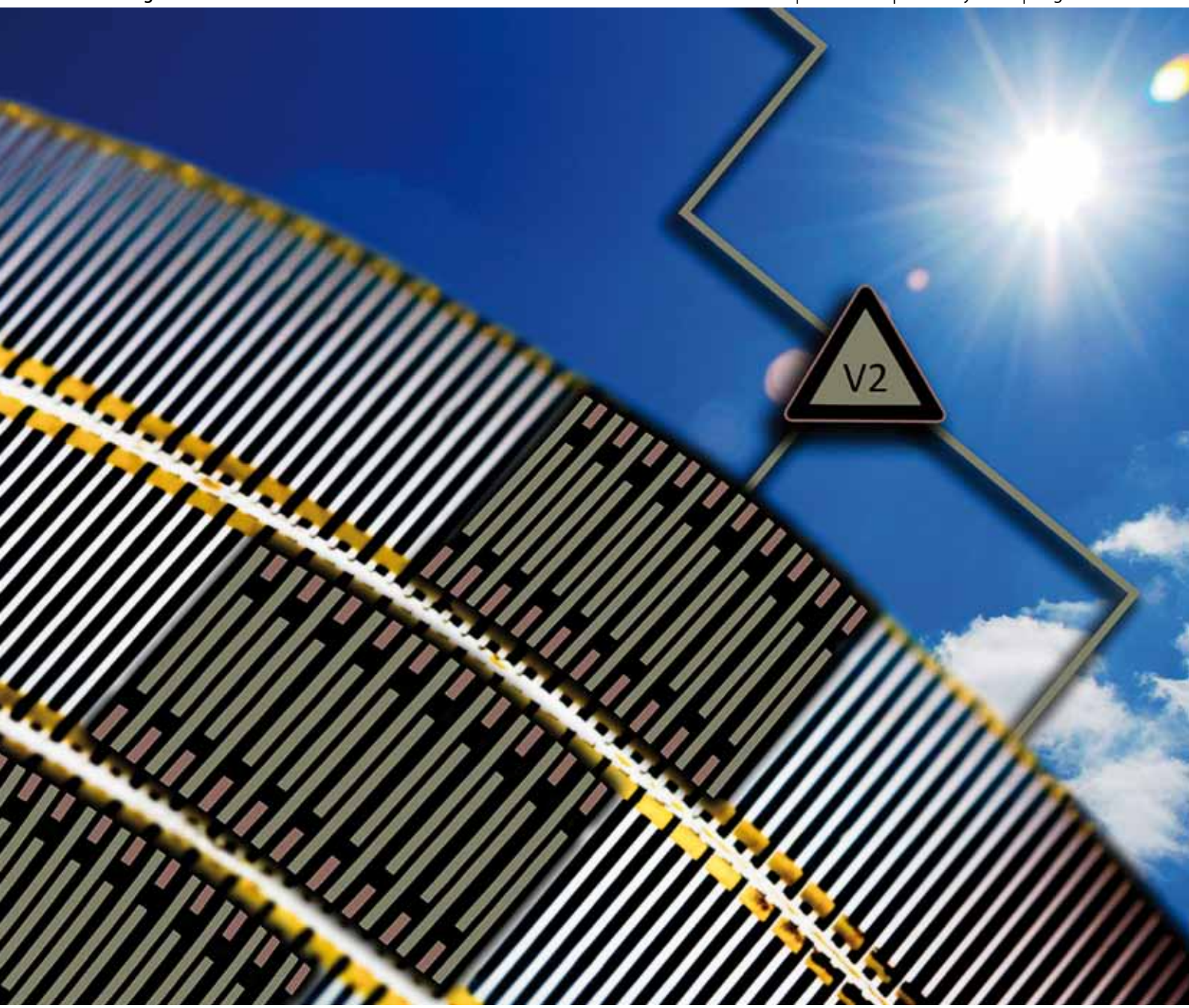

ISSN 1754-5692

COVER ARTICLE
John Rogers *et al*
Compact monocrystalline silicon solar modules with high voltage outputs and mechanically flexible designs

REVIEW
David King *et al*
Biofuels and synthetic fuels in the US and China: A review of Well-to-Wheel energy use and greenhouse gas emissions with the impact of land-use change

RSC Publishing

Compact monocrystalline silicon solar modules with high voltage outputs and mechanically flexible designs

Alfred J. Baca,†[a] Ki Jun Yu,†[b] Jianliang Xiao,[c] Shuodao Wang,[c] Jongseung Yoon,[d] Jae Ha Ryu,[b] Darren Stevenson,[a] Ralph G. Nuzzo,[a] Angus A. Rockett,[d] Yonggang Huang[c] and John A. Rogers*[abd]

Received 7th October 2009, Accepted 15th December 2009
First published as an Advance Article on the web 11th January 2010
DOI: 10.1039/b920862c

A type of compact (~cm^2) high voltage photovoltaic module that utilizes large collections of ultrathin (~15 μm), small (~45 μm wide, ~1 mm long) silicon solar cells was fabricated and characterized. Integration on thin sheets of plastic yielded flexible modules with per-cell efficiencies of ~8%, voltage outputs >200 V, and maximum power outputs >1.5 mW.

In the past several years the photovoltaic (PV) market has experienced rapid growth, with Si (in various crystalline forms) forming the basis of ~90% of the installed modules.[1] Enhancing the conversion efficiency of non-crystalline Si,[2] reducing the usage of Si per unit power output[3] and relaxing purity[4] requirements on Si feedstock represent some priorities for research. Routes for reducing silicon usage and facilitating large area processing, both with the potential to lower costs, include use of ultrathin layers of either amorphous or microcrystalline Si.[5] The main disadvantage of these approaches is the diminished performance of the associated solar cells compared to similar devices formed with monocrystalline Si. One alternative strategy to large-area, materials-efficient cells, relies on anisotropic etching procedures to create thin 'slivers' of Si from bulk wafers, followed by mechanical manipulation to produce modules.[6] Recently, we reported a complementary approach that first creates ultrathin bars, membranes or ribbons of Si from the near surface of a wafer. This scheme uses procedures originally developed for thin Si electronic devices,[7,8] and assembles the elements, each configured as a separate, functional solar cell (*i.e.* a microcell, or μ-cell), in ordered arrays on a target substrate by use of a soft printing process.[3] These techniques allow for the fabrication of compact modules out of hundreds or thousands of such μ-cells, with good efficiencies and the capacity to exploit Si in unconventional module designs. Examples include mechanically flexible and stretchable formats, semitransparent layouts, and ultralow profile microconcentrator designs.

An important additional feature of the μ-cell module construction is the relative ease with which the outputs can be configured for high voltage. Such layouts can be important for driving devices that require high (*e.g.* microelectromechanical systems and certain classes of electronic paper technologies) or even moderate voltage (*e.g.* logic circuits), and they can also be exploited to reduce series resistance losses. Recent reports describe small scale modules with high voltage outputs based on thin films of polymer[9] and crystalline Si[10] as active materials. The former case employs a structured design that offers the possibility for cost effective, mechanically flexible modules, but with efficiency and long term reliability limited by the polymers. The latter example involves the use of a rigid, silicon-on-insulator wafer whose cost is unlikely to be compatible with most applications. Neither system offers the combination of small scale design, robust high performance operation and mechanical properties required of some of the most demanding (*i.e.* mechanically) or otherwise interesting applications.

[a]*Fredrick Seitz Materials Research Laboratory, Beckman Institute, Department of Chemistry, University of Illinois at Urbana-Champaign, Urbana, Illinois, 61801, USA. E-mail: jrogers@illinois.edu; Fax: +217 333 2736; Tel: +217 244 4979*
[b]*Department of Electrical and Computer Engineering, University of Illinois at Urbana-Champaign, Urbana, Illinois, 61801, USA*
[c]*Department of Mechanical Engineering, Northwestern University, Evanston, Illinois, 60208, USA*
[d]*Department of Material Science and Engineering, University of Illinois at Urbana-Champaign, Urbana, Illinois, 61801, USA*
† These authors contributed equally to this work.

Broader context

Silicon continues to represent one of the most compelling materials for solar energy conversion; it remains the dominant choice for commercial photovoltaic applications. Research in this area focuses mainly on enhancing the conversion efficiency of non-crystalline Si, reducing the materials usage per unit power output and relaxing the requirements on purity. Thin films of amorphous or microcrystalline Si and thin sheets of single crystalline Si represent the most widely explored routes to efficient materials utilization. Recently, we reported an alternative strategy that involves production of ultrathin and small Si solar cells (*i.e.* μ-cells) from bulk, commodity wafers by use of lateral anisotropic etching techniques, followed by assembly of these μ-cells into interconnected arrays by use of soft transfer printing methods. Here we describe minimodules that exploit large collections of such μ-cells printed to allow series electrical interconnection for compact modules (~2 cm^2) that are capable of producing high voltage outputs. When formed on thin sheets of plastic in optimized neutral mechanical plane designs, these modules can bend to radii of curvature as small as ~2 mm without any measurable changes in the electrical properties. These devices provide a relatively simple route to low-cost, high-voltage flexible photovoltaic devices, suitable for portable and wearable electronic applications.

The fabrication for the μ-cells reported here uses processes whose details are described elsewhere.[3] Briefly, the process began with a p-type (111) Czochralski Si wafer (3 inch diameter, 1–10 Ω cm, 450 μm thickness, Virginia Semiconductor) coated with a layer of SiO_2 (600 nm) formed by plasma-enhanced chemical vapour deposition (PlasmaTherm SLR). The SiO_2 was lithographically patterned to expose regions of the Si in narrow parallel stripes. Inductively coupled plasma reactive-ion etching (STS ICP-RIE) formed trench structures in the Si,[8] with typical depths of 15–20 μm and widths of 45 μm. Selective doping of emitter and bottom contact areas used solid-state sources of boron (BN-1250, Saint Gobain) and phosphorus (PH-1000N, Saint Gobain) at 1000 °C under N_2 atmosphere for 30 min (boron) and 10 min (phosphorus). Protecting the top surfaces and sidewalls with a bilayer SiO_2/Si_3N_4 mask followed by immersion in a KOH bath resulted in undercut etching of the μ-cells, leaving them tethered to the underlying wafer only at their end points and ready for printing and integrating into modules.

Light and dark current–voltage (*I–V*) measurements of μ-cells were carried out at room temperature using a d.c. source meter (model 2400, Keithley) and a 1000 W full-spectrum solar simulator. For individual cells the reported figures of merit are based on their spatial dimensions, without accounting for coupling of light through the edges. Module level efficiencies are reported using both the aperture area (*i.e.*, includes blank spaces between the cells; 0.95 cm × 0.63 cm) and the active area (*i.e.*, only the silicon area exposed to incoming flux; 0.50 cm × 0.57 cm). In all cases, we used a diffusive backside reflector during measurements. Contributions due to light flux from diffuse illumination and inter-cell areas is an inherent feature of the design that improves the power output per unit area of active device. Electrical characterization of performance during bending involved mounting complete modules on glass tubes with radii of curvature of 4 mm. Fatigue tests were also performed, where one cycle corresponds to bending a module to a given radius and then relaxing it to a flat state.

Fig. 1a shows a scanning electron microscope (SEM) image of partially undercut μ-cells, tethered to the host wafer *via* anchor points at their ends; the widths, lengths and thicknesses are ~45 μm, ~1.5 mm and ~15 μm, respectively. The inset provides a high magnification cross-sectional view of an individual μ-cell. The μ-cell layouts were fabricated such that p^+ and n^+ doped regions alternate from cell to cell, as shown in the colorized SEM image in Fig. 1b. The green, red and grey areas represent phosphorus doped (1.30 mm long), boron doped (0.15 mm long), and un-doped Si regions (0.05 mm long), respectively. This design provides access for top side contacts, thereby facilitating the wiring of individual cells for metal interconnection in series, in a monolithic fashion.

Fig. 2a provides a schematic illustration of transfer printing μ-cells (*via* an elastomeric stamp; PDMS) for integration into modules. The μ-cells are tethered onto the host wafer *via* anchor points[11] as illustrated in Fig. 2b. Placing the PDMS stamp on the surface of the μ-cells, followed by quickly lifting the stamp,[12] removed the μ-cells from the host wafer (Fig. 2c). Insets in Fig. 2b and c show close up views of the anchor regions before and after retrieval of the stamp, respectively. The PDMS stamp was used to print the cells onto a layer (~30μm) of photocurable polyurethane (NOA 61; Norland Optical Adhesive) spin coated onto a glass slide (carrier substrate). Metallization *via* sputter coating of Cr/Au (5/600 nm) followed by photolithography and etching of the exposed metal defined interconnect

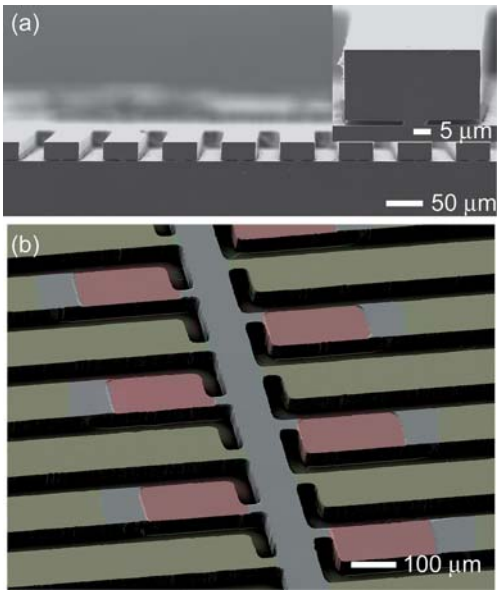

Fig. 1 (a) SEM cross-sectional view of partially undercut microcells. Inset shows a high magnification cross-sectional view of an individual μ-cell. (b) Colorized SEM image of an array of microcells on a source wafer, ready for printing illustrating the selective doping areas and microcell layout. Green regions correspond to phosphorous doped areas (n^+), red regions are boron doped areas (p^+), and gray areas are un-doped Si.

wiring. For flexible systems, a second layer of NOA (30 μm thick) cast on top of the printed arrays placed the fragile elements (*i.e.*, metal and Si) close to the neutral mechanical plane of modules completed by removal from the carrier substrate. Fig. 2d illustrates a module consisting of 768 μ-cells connected in series. The metallization factor for this layout is ~16%, defined as the fraction of device area covered in an individual microcell.

Fig. 3a provides a high resolution SEM image of a section of the high voltage minimodule which indicates the device layout. Fig. 3b shows the *IV* characteristics of a typical, individual μ-cell. The solar conversion efficiency varied between 6–8% with open circuit voltages (V_{oc}) between 0.44–0.48 V, current densities (J_{SC}) of 23–26 mA cm^{-2}, maximum power (P_{max}) output of 3–4 μW and fill factors of 0.67–0.68. Efficiencies in the current devices are limited by low J_{SC} and V_{oc} values possibly due to carrier recombination at the metal contacts. Fig. 3c shows the *IV* characteristics for a different number of rows composed of μ-cells (128 μ-cells per row) connected in series. An individual row fabricated in this way shows maximum voltage and power outputs of ~51 V and 0.37 mW, respectively. As shown in Fig. 3c, increasing the number of rows leads to systematic and expected changes in the characteristics, with voltage outputs of 51 V, 104 V, 155 V and 209 V for 1, 2, 3 and 4 rows, respectively. Si solar cells with conventional dimensions would require much larger areas to generate the voltages produced here. The inset in Fig. 3c shows the maximum power (1.55 mW) from a 0.95 cm × 0.63 cm module composed of 512 μ-cells. The aperture area and active area efficiency for this minimodule is 2.8% and 5.2%, respectively. Fig. 3d presents the scaling properties of the number of μ-cells interconnected in series and the corresponding voltage and maximum power outputs. The parameters vary in an almost linear fashion with number of cells, as expected. Such arrays of μ-cells can also be wired in parallel for high

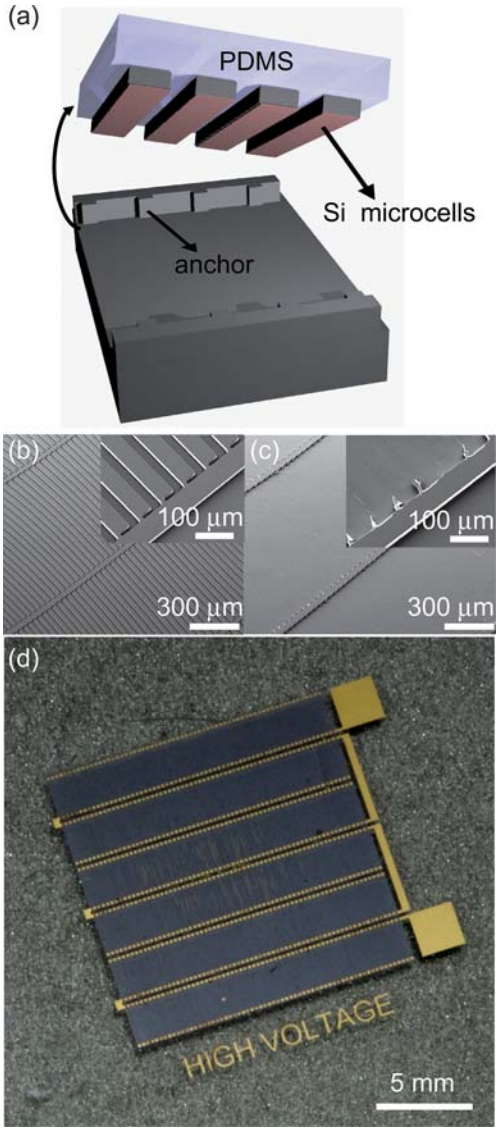

Fig. 2 (a) Schematic illustration of the transfer printing process used to fabricate high voltage PV minimodules. (b) SEM image of fully undercut μ-cells tethered onto a Si wafer ready for printing. (c) SEM image of the Si wafer after retrieval of the μ-cells. Insets in (b) and (c) shows close up views of the anchor geometries before and after pickup, respectively. (d) Optical image of a completed minimodule consisting of printed microcell arrays interconnected in series by Cr/Au lines.

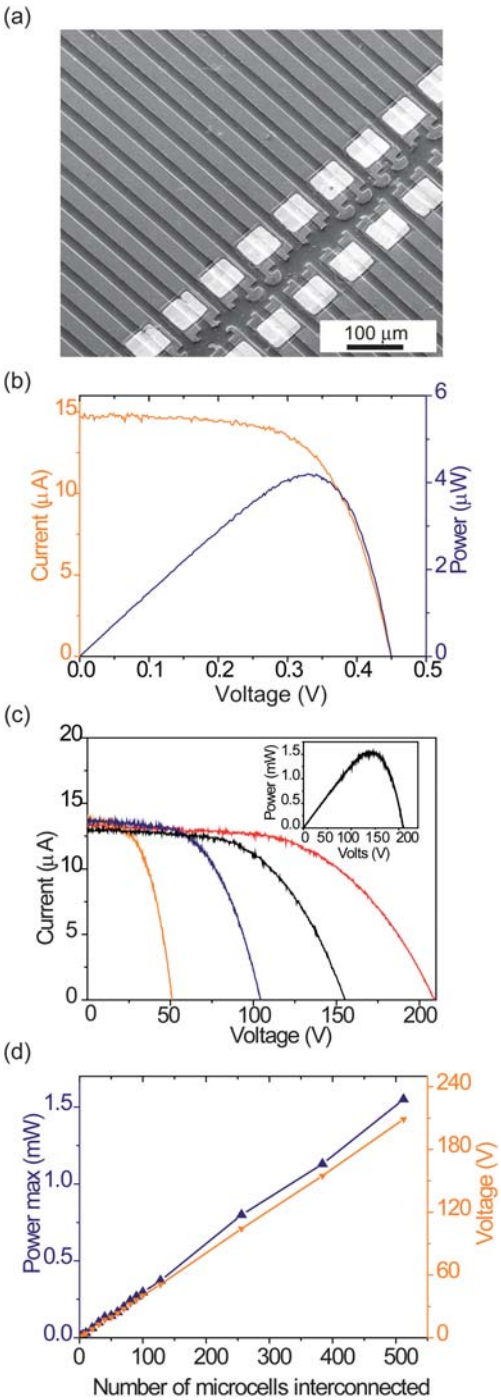

Fig. 3 (a) SEM image of a section of a high voltage minimodule. The lighter regions (rectangular features) in (a) correspond to the Au metal contacts. (b) Current–voltage characteristics of an individual Si microcell. (c) Current–voltage characteristics of rows of Si microcells interconnected in series from left to right: 1 row (orange), 2 rows (blue), 3 rows (black) and 4 rows (red). Inset depicts the maximum power output of 512 microcells. (d) Scaling properties for voltage and power outputs of different numbers of microcells interconnected in series.

current applications, therefore allowing for a wide range of voltage and current requirements depending on the target application.

A unique aspect of the printing approach to integration is the ability to assemble μ-cells on sheets of plastic, in a scalable, deterministic and high throughput manner, for the fabrication of flexible and rollable PV modules, in optimized neutral mechanical layouts. Fig. 4a shows an optical image of a high voltage flexible PV module conformally wrapped around a glass tube with a radius of curvature of ~7 mm. For a unit cell as shown in the inset of Fig. 4b, analytical modeling gives the strain at position z as $\varepsilon = (z - z_0)/R$ for bending perpendicular (y-direction) to the interconnect direction, where R is the bending radius, $z_0 = a - t/2 - (1/2)(a + b)(a - t - b)/[a + b + t(E_{Si}/E_{NOA} - 1)W_{Si}/W]$ is the position of neutral mechanical plane, E_{Si} and E_{NOA} are the Young's moduli of Si and NOA, and a, b, t, W_{Si} and W are the geometry parameters as shown in the inset of Fig. 4b.[3] The maximum strain in the Si is

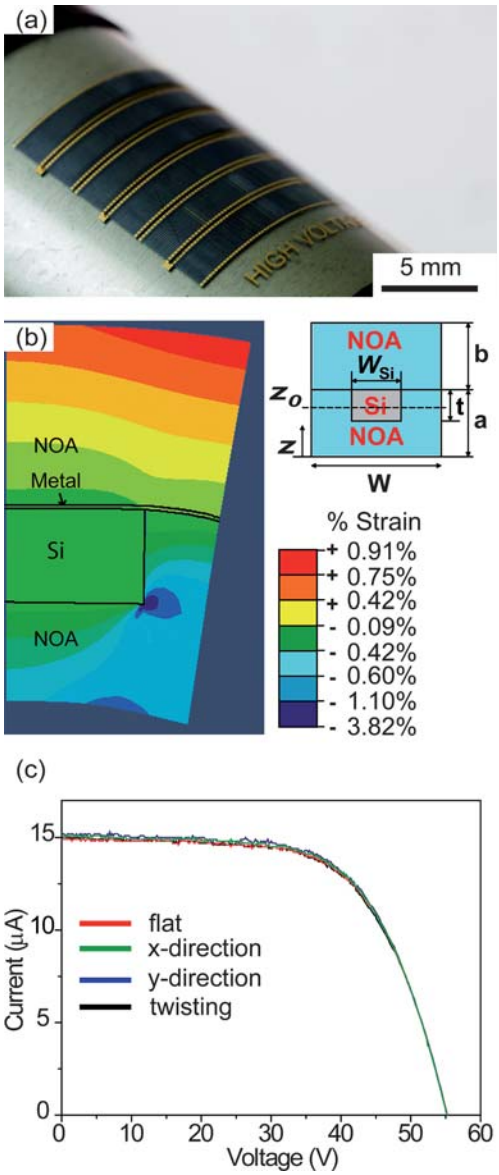

Fig. 4 (a) Optical micrograph of a flexible high voltage module conformally wrapped around a glass tube. (b) Color contour plot of calculated bending strains (ε_{xx}; bending strain of NOA/Si along the interconnect direction) through a cross-section of a high voltage minimodule, bent outward along the cell width direction at a bending radius of 4 mm. Inset depicts the unit cell of the flexible modules, which is used to deduce the analytical modeling results. (c) Current–voltage characteristics of a high voltage minimodule in a flat state, bent along the microcell width microcell length, and under a twisting deformation (45°).

$$\varepsilon_{\max}^{Si} = \frac{t}{2R}\max\left[\left|1+\frac{a-t-b}{t+\frac{t^2}{a+b}\left(\frac{E_{Si}}{E_{NOA}}-1\right)\frac{W_{Si}}{W}}\right|, \left|1-\frac{a-t-b}{t+\frac{t^2}{a+b}\left(\frac{E_{Si}}{E_{NOA}}-1\right)\frac{W_{Si}}{W}}\right|\right] \quad (1)$$

Since the metal is very thin, its strain approximately equals the strain at the top surface of Si and is obtained as

$$\varepsilon_{\max}^{metal} = \frac{t}{2R}\left[1+\frac{a-t-b}{t+\frac{t^2}{a+b}\left(\frac{E_{Si}}{E_{NOA}}-1\right)\frac{W_{Si}}{W}}\right] \quad (2)$$

Based on experimental structures and geometry layouts, maximum strains in the μ-cells and metal interconnects are less than 0.4% for bending radii of 2 mm perpendicular (*y*-direction) to the interconnect direction.[3] Fig. 4b presents finite element modeling of the distribution of strain for outward bending to a radius of curvature of 4 mm along (*x*-direction) the interconnect direction, while Fig. 4c shows the *IV* characteristics of such modules in a flat state (un-bent), bent along (*x*-direction) and perpendicular (*y*-direction) to the interconnect direction and under a twisting deformation (45°). The results in Fig. 4c and mechanical fatigue test of up to 1000 cycles show little or no changes in the *IV* characteristics consistent with the analytical modeling results.

In conclusion, this work demonstrates a compact Si solar module capable of producing high voltage outputs in mechanically flexible designs. Demonstration experiments show voltage and power outputs of >200 V and >1.5 mW, respectively, and bendability to radii of curvature down to 4 mm without significant changes in the solar cell figures of merit. These results illustrate some advantages of modules that rely on μ-cells and printing based assembly techniques.

Acknowledgements

A.J.B. acknowledges support from the Department of Defense Science, Mathematics and Research for Transformation (SMART) fellowship. We thank T. Banks for help with processing. We acknowledge support by the US Department of Energy (DoE), Division of Materials Sciences, under award DE-FG02-07ER46471, through the Materials Research Laboratory (MRL). Y.H. acknowledges the support from ISEN, Northwestern University.

Notes and references

1 D. M. Bagnall and M. Boreland, *Energy Policy*, 2008, **36**, 4390.
2 Y. Sobajima, S. Nakano, M. Nishino, Y. Tanaka, T. Toyama and H. Okamoto, *J. Non-Cryst. Solids*, 2008, **354**, 2407.
3 J. Yoon, A. J. Baca, S. I. Park, P. Elvikis, J. B. Geddes, L. F. Li, R. H. Kim, J. L. Xiao, S. D. Wang, T. H. Kim, M. J. Motala, B. Y. Ahn, E. B. Duoss, J. A. Lewis, R. G. Nuzzo, P. M. Ferreira, Y. G. Huang, A. Rockett and J. A. Rogers, *Nat. Mater.*, 2008, **7**, 907.
4 S. Pizzini, *Appl. Phys. A: Mater. Sci. Process.*, 2009, **96**, 171.
5 L. V. Mercaldo, M. L. Addonizio, M. Della Noce, P. D. Veneri, A. Scognamiglio and C. Privato, *Appl. Energy*, 2009, **86**, 1836.
6 K. J. Weber and A. W. Blakers, (Aranda, Australia), Australian National University, ACT, Australia, 10432936 PCT/AU01/01546, Nov 2001, *Appl. #11/193,183*, 29 July 2005; P. J. Verlinden, A. W. Blakers, K. J. Weber, J. Babaei, V. Everett, M. J. Kerr, M. F. Stuckings, D. Gordeev and M. J. Stocks, *Sol. Energy Mater. Sol. Cells*, 2006, **90**, 3422.
7 A. J. Baca, J. H. Ahn, Y. Sun, M. A. Meitl, E. Menard, H. S. Kim, W. M. Choi, D. H. Kim, Y. Huang and J. A. Rogers, *Angew. Chem., Int. Ed.*, 2008, **47**, 5524; H. C. Ko, A. J. Baca and J. A. Rogers, *Nano Lett.*, 2006, **6**, 2318.
8 A. J. Baca, M. A. Meitl, H. C. Ko, S. Mack, H. S. Kim, J. Y. Dong, P. M. Ferreira and J. A. Rogers, *Adv. Funct. Mater.*, 2007, **17**, 3051.
9 M. Niggemann, W. Graf and A. Gombert, *Adv. Mater.*, 2008, **20**, 4055.
10 P. Ortega, S. Bermejo and L. Castaner, *Progr. Photovolt.: Res. Appl.*, 2008, **16**, 369.
11 M. A. Meitl, X. Feng, J. Y. Dong, E. Menard, P. M. Ferreira, Y. G. Huang and J. A. Rogers, *Appl. Phys. Lett.*, 2007, **90**, 083110.
12 M. A. Meitl, Z. T. Zhu, V. Kumar, K. J. Lee, X. Feng, Y. Y. Huang, I. Adesida, R. G. Nuzzo and J. A. Rogers, *Nat. Mater.*, 2006, **5**, 33.